

Theoretical and experimental studies of relativistic oversized Ka-band surface-wave oscillator based on 2D periodical corrugated structure

N. S. Ginzburg,^{1,2} E. V. Ilyakov,¹ I. S. Kulagin,¹ A. M. Malkin,¹ N. Yu. Peskov,^{1,2}
A. S. Sergeev,¹ and V. Yu. Zaslavsky^{1,2}

¹*Institute of Applied Physics, Russian Academy of Sciences, Nizhny Novgorod, 603950 Russia*

²*Nizhny Novgorod State University, Nizhny Novgorod, 603950 Russia*



(Received 9 April 2018; published 7 August 2018)

Based on a quasioptical approach and direct particle-in-cell simulations, we study dynamics of oversized relativistic surface-wave oscillators (SWOs) of the Cherenkov type with 2D periodical corrugated structures of cylindrical geometry. Such corrugation allows significant rarefaction of the spectrum of modes with different azimuthal indices. As a result, selective excitation of a mode with a given azimuthal index is possible. Azimuthal index of the generated mode depends on the voltage rise time. For short (nanosecond scale) rise time, generation of an azimuthally symmetric mode can be realized. For longer (hundreds nanoseconds to microseconds) rise time, the modes with high azimuthal indexes would be excited. These conclusions are supported by the experiments where Ka-band SWOs with 2D corrugated structures were realized based on the 300 keV/100 A/4 μ s thermionic accelerator SATURN. For an oversize factor of 16, stable narrow-band generation with output power of 1.5–2 MW was obtained at the frequency of 32.5 GHz corresponding to the mode with an azimuthal index of $m = 3$. The project of Ka-band subgigawatt power SWOs operating at the azimuthally symmetric mode based on 500 keV/4 kA/20 ns high current explosive-emission accelerator SINUS-6 is under development.

DOI: [10.1103/PhysRevAccelBeams.21.080701](https://doi.org/10.1103/PhysRevAccelBeams.21.080701)

I. INTRODUCTION

For spatially extended relativistic electron beams of sheet and tubular geometry, the use of two-dimensional (2D) distributed feedback is beneficial for providing spatial coherence of radiation and can be exploited in order to increase the total radiation power in the microwave generators [1,2]. Such 2D feedback can be realized in planar and coaxial 2D Bragg structures (resonators) having double-periodic corrugation. Experimental studies of free electron masers (FEMs) based on the novel feedback mechanism have been performed in Ka-band (coaxial geometry) at the University of Strathclyde (Glasgow, UK) [3] and in W-band (planar geometry) at the Budker Institute of Nuclear Physics (Novosibirsk, Russia) [4,5] in collaboration with the Institute of Applied Physics RAS. As a result, narrow-band generation with an output power on the level of 50–100 MW, which is a record for millimeter wavelength FEMs, was obtained.

At present, theoretical [6–8] and experimental [8,9] studies of Cherenkov masers with 2D distributed feedback

are in progress. Among relativistic masers of such type, surface wave oscillators (SWOs) [10–18] appear to be preferable due to the larger values of the electron-wave coupling impedance. Besides, formation of a surface mode ensures the regular field distribution along the coordinate directed perpendicularly to the corrugated surface and, thus, can solve the problem of mode selection over this coordinate. In SWOs, a 2D periodic structure can be exploited both as a slow-wave system and as a highly selective Bragg resonator simultaneously [19,20]. It provides effective mode control over azimuthal coordinate.

The present paper is devoted to theoretical and experimental studies of the oversized cylindrical SWOs with 2D periodical corrugated structure (2D SWOs). Simulations of nonlinear dynamics of the oscillator were performed both in the frame of quasioptical approach and by using the CST STUDIO SUITE particle-in-cell (PIC) code. Simulation parameters were chosen close to those of the experimental setups. The paper is organized as the follows. In Sec. II, a quasioptical model describing SWOs with 2D periodical grating is formulated and mode dynamics of the generators of such type are studied. In Sec. III, results of direct PIC simulations of a Ka-band 2D SWOs based on the thermionic-emission accelerator SATURN (IAP RAS) are presented in comparison with experimental investigations. Section IV contains results of simulations of sub-GW power level Ka-band 2D SWOs based on the explosive-emission accelerator SINUS-6 (IAP RAS).

Published by the American Physical Society under the terms of the Creative Commons Attribution 4.0 International license. Further distribution of this work must maintain attribution to the author(s) and the published article's title, journal citation, and DOI.

II. QUASIOPTICAL MODEL OF SWO WITH 2D PERIODICAL GRATING

To study nonlinear dynamics of SWOs based on the oversized cylindrical waveguide with 2D periodical grating, we assume that a hollow rectilinear electron beam moves along the grating with a longitudinal velocity of $v_0 = \beta_0 c$ [Fig. 1(a)]. The surface of the waveguide is corrugated as

$$r = \frac{\tilde{r}}{4} [\cos(\bar{M}\varphi - \bar{h}_z z) + \cos(\bar{M}\varphi + \bar{h}_z z)] \quad (1)$$

and represents a superposition of two helical gratings with opposite rotations, where \tilde{r} is the corrugation depth, $\bar{h}_z = 2\pi/d_z$, d_z is the corrugation period along the longitudinal coordinate z and \bar{M} is the number of variations (turns) of the corrugation over the azimuthal coordinate φ . We assume that the system parameters satisfy the following relation:

$$\bar{h}_z \approx \bar{h}_x = \bar{h}, \quad (2)$$

where $\bar{h}_x = \bar{M}/r_0$. If the curvature of the waveguide is small, i.e. the conductor radius r_0 is substantially larger than the radiation wavelength λ , it is appropriate to introduce a new azimuthal coordinate $x = r_0\varphi$ and to use the quasiplanar model for description of the waves coupling. In this model, the radial y coordinate is directed normally to the surface of the conductor.

Within the described model, the electromagnetic field confined at the grating (1) is formed by the four partial wave beams with the following components of the magnetic field [20]:

$$\begin{aligned} H_x &= \text{Re}\{(C_z^+ e^{-ihz} + C_z^- e^{ihz})e^{i\omega t}\}, \\ H_z &= \text{Re}\{(C_x^+ e^{-ihx} + C_x^- e^{ihx})e^{i\omega t}\}, \end{aligned} \quad (3a)$$

where $C_{x,z}^\pm(x, y, z, t)$ are the slow functions of the coordinates and time, \vec{x}_0 , \vec{y}_0 and \vec{z}_0 are the coordinate unity vectors. Two of these beams C_z^\pm are propagating in the

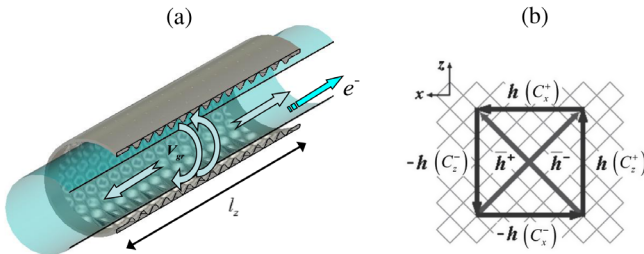


FIG. 1. (a) Scheme of an oversized SWO with 2D corrugated structure. Directions of propagation of the partial wave fluxes and tubular electron beam are shown. (b) Diagram illustrating coupling of partial waves at the 2D corrugation.

longitudinal $\pm z$ -directions and the other two C_x^\pm are propagating in the transverse (azimuthal) $\pm x$ ($\pm\varphi$) directions. Electric fields are expressed from (3a) as

$$\begin{aligned} E_x &= \frac{c}{\omega} \text{Im} \left[\left(\frac{\partial C_x^+}{\partial y} e^{-ihx} + \frac{\partial C_x^-}{\partial y} e^{ihx} \right) e^{i\omega t} \right], \\ E_z &= -\frac{c}{\omega} \text{Im} \left[\left(\frac{\partial C_z^+}{\partial y} e^{-ihx} + \frac{\partial C_z^-}{\partial y} e^{ihx} \right) e^{i\omega t} \right], \\ E_y &= \frac{c}{\omega} \text{Im} \left\{ \left[\left(-ihC_z^+ - \frac{\partial C_x^+}{\partial x} \right) e^{-ihz} \right. \right. \\ &\quad \left. \left. + \left(ihC_z^- - \frac{\partial C_x^-}{\partial x} \right) e^{ihz} \right] e^{i\omega t} \right\}. \end{aligned} \quad (3b)$$

Under the Bragg resonance condition

$$h \approx \bar{h} \quad (4)$$

longitudinal C_z^\pm and azimuthal C_x^\pm wave fluxes are coupled to each other as shown in Fig. 1(b) where an unfolded corrugated surface with the directions of the partial wave beams propagation is depicted.

Having chosen the Bragg frequency $\bar{\omega} = \bar{h}c$ for a reference one, we describe the excitation of the surface waves by the electron beam using the equations similar to those formulated in [20]:

$$\begin{aligned} \left(\frac{\partial}{\partial \tau} + \frac{\partial}{\partial Z} + i \frac{\partial^2}{\partial Y^2} \right) \hat{C}_z^+ + i\alpha(\hat{C}_x^+ + \hat{C}_x^-) \delta(Y) \\ = -\frac{1}{B_e} \frac{\partial}{\partial Y} \left(J F_e(Y) \right), \\ \left(\frac{\partial}{\partial \tau} - \frac{\partial}{\partial Z} + i \frac{\partial^2}{\partial Y^2} \right) \hat{C}_z^- + i\alpha(\hat{C}_x^+ + \hat{C}_x^-) \delta(Y) = 0, \\ \left(\frac{\partial}{\partial \tau} \pm \frac{\partial}{\partial X} + i \frac{\partial^2}{\partial Y^2} \right) \hat{C}_x^\pm + i\alpha(\hat{C}_z^+ + \hat{C}_z^-) \delta(Y) = 0, \end{aligned} \quad (5)$$

where $\delta(Y)$ is the delta function, $F_e(Y)$ is a function expressing the radial current density of the electron beam with an effective thickness of $B_e = \int_0^{R_0} F_e(Y) dY$. Amplitude of the rf current $J = \frac{1}{\pi} \int_0^{2\pi} e^{-i\theta} d\theta_0$ can be found from the electron motion equations

$$\left(\frac{1}{\beta_0} \frac{\partial}{\partial \tau} + \frac{\partial}{\partial Z} \right)^2 \theta = \text{Re} \left[\frac{\partial \hat{C}_z^+}{\partial Y} e^{i\theta} \right], \quad (6)$$

with the boundary conditions

$$\theta|_{Z=0} = \theta_0 \in [0; 2\pi), \quad \left. \left(\frac{1}{\beta_0} \frac{\partial}{\partial \tau} + \frac{\partial}{\partial Z} \right) \theta \right|_{Z=0} = \Delta. \quad (7)$$

Here $\theta = \bar{\omega}(t - z/c)$ is the electron phase with respect to the forward partial wave C_z^+ , $\Delta = (1 - \beta_0)/\beta_0 G > 0$ is the synchronism detuning at the carrier Bragg frequency

varying with changes in the particle energy. The synchronous interaction with a rectilinear electron beam arises due to the formation of an evanescent slow wave. In Eqs. (5)–(7), we introduced the following normalized variables and parameters: $Z = G\bar{h}z$, $X = G\bar{h}x$, $Y = \sqrt{2G\bar{h}}y$, $\tau = G\bar{\omega}t$, $\hat{C}_{x,z}^{\pm} = \frac{e\mu C_{x,z}^{\pm}}{mc\bar{\omega}\gamma_0 G^{3/2}}$,

$$G = \left(\frac{\sqrt{2}\mu\lambda I_0}{\pi\gamma_0 r_0 I_a} \right)^{2/3} \quad (8)$$

is the gain parameter, $I_a = mc^3/e$, I_0 is the total electron beam current, $\mu \approx \gamma_0^{-2}\beta_0^{-3}$ is the electron bunching parameter, $\alpha = \frac{\bar{h}\bar{r}}{8G}$ is normalized wave coupling parameter at the corrugation, $\gamma_0 = (1 - \beta_0^2)^{-1/2} = 1 + \frac{eU}{mc^2}$ is the relativistic mass factor depending on accelerating voltage U .

Due to the cylindrical geometry of the cavity, the wave-beam amplitudes satisfy the cyclic boundary conditions

$$\hat{C}_{x,z}^{\pm}(X + L_x, Y, Z, \tau) = \hat{C}_{x,z}^{\pm}(X, Y, Z, \tau), \quad (9)$$

where $L_x = 2\pi\bar{h}Gr_0$ is perimeter of the structure. Condition (9) allows a solution of Eq. (5) to be expanded in a Fourier series,

$$\hat{C}_{x,z}^{\pm}(X, Y, Z, \tau) = \sum_{m=-\infty}^{+\infty} \hat{C}_{x,z}^{\pm;m}(Y, Z, \tau) e^{i\Gamma_x^m X}, \quad (10)$$

and consider each harmonic as a mode with an azimuthal index of m , where $\Gamma_x^m = 2\pi m/L_x$ is the azimuthal wave number of the m th mode.

In the absence of the electron beam [zero right hand part of the first equation in the system of Eqs. (5)] assuming that the radius of the waveguide is sufficiently large in the scale of the surface mode radial decay and presenting solutions of Eq. (5) at $y > 0$ as

$$\hat{C}_{x,z}^{\pm;m} \sim \exp(i\Omega_m \tau \mp i\Gamma_z z - g_{x,z}^{\pm;m} Y), \quad (11)$$

we get the following dispersion relation for partial waves in a 2D Bragg slow-wave structure unbounded in the longitudinal direction (see [20] for details):

$$\alpha^2 \left(\frac{1}{g_z^{+;m}} + \frac{1}{g_z^{-;m}} \right) \left(\frac{1}{g_x^{+;m}} + \frac{1}{g_x^{-;m}} \right) = 1, \quad (12)$$

where

$$g_z^{\pm;m} = \sqrt{-\frac{\Omega_m}{c} \pm \Gamma_z}, \quad g_x^{\pm;m} = \sqrt{-\frac{\Omega_m}{c} \pm \Gamma_x^m} \quad (13)$$

are the radial wave numbers. Family of solutions of (12) and (13) is shown in Fig. 2. Each dispersion curve $\Omega_m(\Gamma_z)$ corresponds to a ‘‘cold’’ mode with an azimuthal index of m . It is important to note that dispersion curves with high

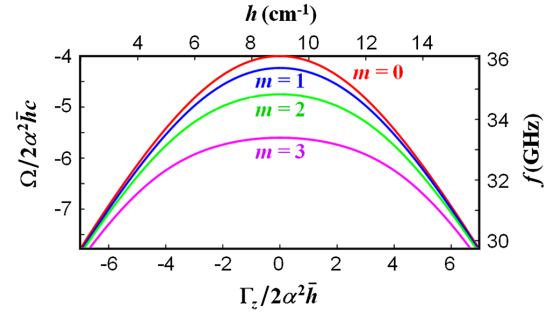


FIG. 2. Dispersion lines of the normal waves with various azimuthal indices m slowed by the 2D corrugation, which were obtained by solving Eq. (12) for the geometrical parameters given in Table I, $f = \omega/2\pi$.

azimuthal indices are located below the curve corresponding to an azimuthally symmetric mode $m = 0$.

For a 2D Bragg structure of finite length L_z , the boundary conditions for Eq. (5) with respect to the z -coordinate set at the edges of the corrugated region correspond to the absence of external energy fluxes

$$\hat{C}_z^+|_{Z=L_z} = 0, \quad \hat{C}_z^-|_{Z=0} = 0, \quad (14)$$

where $L_z = G\bar{h}l_z$ is normalized length of the oscillator. In this case, the spectrum of the eigenmodes contains solutions with various azimuthal and longitudinal indices. Modes with one longitudinal variation possess eigenfrequencies near the highest point of the corresponding dispersion curve and maximal Q-factor. Eigenfrequencies of modes decrease with the increase of azimuthal index m , thus, the azimuthally symmetric mode possesses the highest frequency. It is important to emphasize that due to the presence of the azimuthal energy fluxes, the 2D corrugation allows significant rarefaction of the spectrum of eigenmodes with different azimuthal indices [20]. The frequency interval between the azimuthally symmetric ($m = 0$) and the m th modes increases with m as

$$\Delta\Omega_m = \frac{\Delta\omega_m}{G\omega} \approx \frac{3\pi^2}{8} \frac{m^2}{(\alpha L_x)^2}. \quad (15)$$

For traditional 1D corrugation, the frequency interval corresponding to (15) is given by an expression $\Delta\Omega_m^{1D} \approx 8\pi^2 m^2/L_x^2$ and would be much smaller than the one given by (15) (see [19] for details). This is illustrated by results of CST simulation of excitation of the cylindrical structures having 2D [Fig. 3(a)] and 1D [Fig. 3(b)] corrugations with the same Bragg frequency by an incident short electromagnetic pulse. Field spectra for the first four azimuthal modes are shown in Fig. 3 at the final stage of the decay process. The spectrum bandwidths are proportional to the Q factors of the corresponding modes. Obviously, these factors are practically the same for all modes.

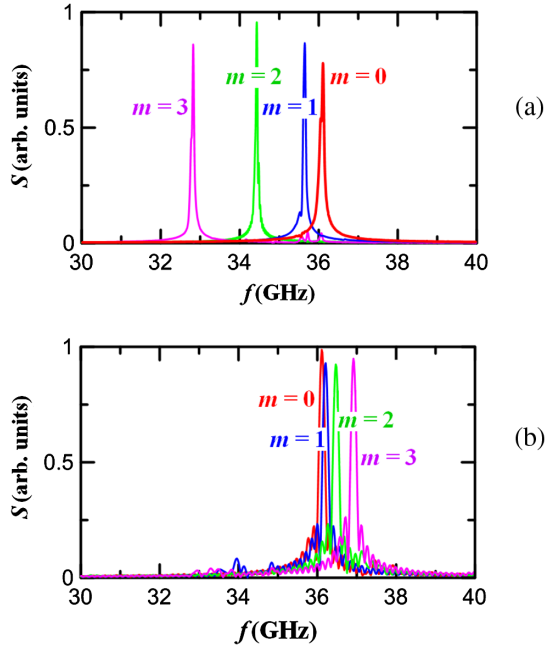


FIG. 3. Field spectra corresponding to excitation of different azimuthal eigenmodes by an initial rf pulse in the cylindrical slow-wave structures having (a) 2D and (b) 1D corrugation (CSR simulations). Parameters of the 2D structure are shown in Table I. Parameters of the 1D structure are as follows: mean cavity radius of 23 mm, length of 87.5 mm, corrugation of the period of 3.5 mm and depth of 1.8 mm.

In the presence of the electron beam [nonzero right hand part of the first equation in the system of Eqs. (5)], Ω_m becomes complex and the eigenmodes are unstable. Figure 4 shows the dependence of the temporal increments $\text{Im}\Omega_m$ and frequency shifts $\text{Re}\Omega_m$ for different azimuthal modes vs the detuning parameter Δ obtained by numerical simulations of the linearized Eq. (5). The maximum increment for a mode with a given index of m is reached under conditions when the beam line crosses the corresponding dispersion curve near its top. Accordingly, at a

relatively large Δ (which corresponds to relatively low particle energies), the maximum increment is reached for modes with high azimuthal index, while the azimuthally symmetric mode would be preferentially excited at higher electron energies.

Such dependence of the increments on the detuning (i.e. on the accelerating voltage amplitude) leads to a fairly complicated mode excitation scenario depending on the voltage pulse rise time. We simulate this pattern using Eqs. (5) and (6) with time-dependent detuning parameter $\Delta(\tau)$ having linear temporal dependence of the front of the voltage pulse and staying constant at the stationary value Δ_{st} after that, i.e.

$$\Delta(\tau) = \begin{cases} \Delta_0 + (\Delta_{st} - \Delta_0) \frac{\tau}{\tau_{\text{rise}}}, & \tau < \tau_{\text{rise}} \\ \Delta_{st}, & \tau \geq \tau_{\text{rise}}. \end{cases} \quad (16)$$

Figure 5 shows the dynamics of buildup of a steady-state oscillation regime set at one of the azimuthal modes depending on the rate of change of the detuning parameter, i.e. on the voltage rise time τ_{rise} . All of the other parameters, including slow-wave system characteristics, beam current and accelerating voltage amplitude, are identical. Figure 5(a) corresponds to the fast voltage rise with azimuthally symmetric mode onset. However, for slower voltage rise, steady state oscillations occur for the modes with higher azimuthal indices [Fig. 5(b)–5(d)]. Even though the detuning reaches the same value of Δ_{st} in all four realizations, the mode excited during the transient suppresses the oscillations at the symmetric mode even under conditions when Δ_{st} corresponds to the maximum increment (minimum starting current) of the latter mode. Simulations demonstrate that the efficiency values of the steady-state oscillations are roughly similar for all operating modes and the regime of excitation of each mode is highly stable with respect to variations of the accelerating voltage amplitude.

Figure 6 illustrates the phase synchronization in the regime of azimuthally symmetric mode excitation

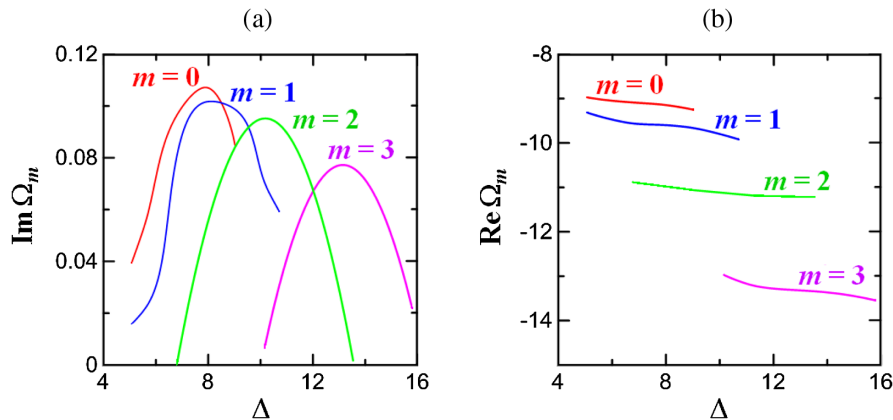


FIG. 4. Temporal increments $\text{Im}\Omega_m$ (a) and eigenfrequencies $\text{Re}\Omega_m$ (b) of the first four azimuthal modes vs detuning parameter Δ for $\alpha = 2.2$, $L_z = 1.5$, $L_x = 1.9$, $B_e = 0.2$.

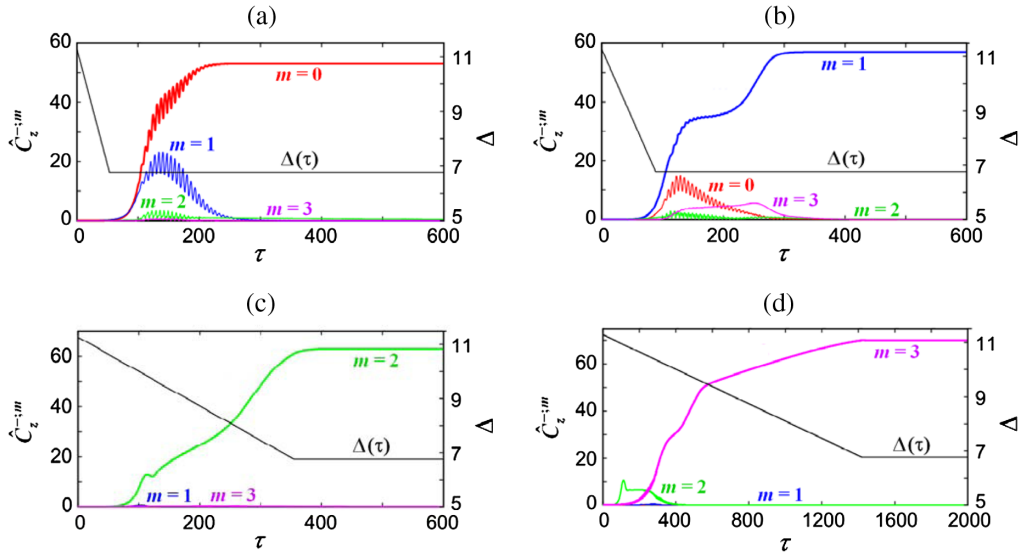


FIG. 5. Scenarios of establishment of the stationary oscillation regime at different azimuthal modes for various fronts of the voltage pulse (rise time). Temporal dependence of the modes amplitudes at the SWO output together with corresponding temporal dependence of the detuning Δ caused by the voltage growing up: (a) $\tau_{\text{rise}} = 50$, (b) $\tau_{\text{rise}} = 80$, (c) $\tau_{\text{rise}} = 350$, (d) $\tau_{\text{rise}} = 1400$; $\alpha = 2.2$, $\Delta_{st} = 8$, $L_z = 1.5$, $L_x = 1.9$, $B_e = 0.2$.

corresponding to Fig. 5(a). The initial phase of the field was set randomly [Fig. 6(a)]. Due to the presence of azimuthal energy fluxes C_x^\pm , rather fast synchronization of emission from different parts of the oversized hollow electron beam is observed. As a result, phase and amplitude become almost constant along the azimuthal coordinate [Fig. 6(b)].

According to the analysis carried out, in a certain range of voltage rise times, one can choose an azimuthal mode, at which the stable oscillations regime could be obtained. This conclusion is verified by Sec. III which presents results of PIC simulation of SWOs with parameters close to the experimental realization based on the accelerator SATURN with thermionic emission cathode having relatively long (about few hundreds nanoseconds) front of voltage pulse. In the correspondence with experiments these simulations demonstrate the excitation of nonsymmetric modes. In Sec. IV, results of PIC simulations of similar oscillator powered by electron beam corresponding to the accelerator SINUS-6 with explosive emission cathode and fast (few nanoseconds) front of the voltage pulse are presented. In

this case, the steady-state oscillations regime occurs for the azimuthally symmetric mode.

III. 3D PIC SIMULATIONS AND EXPERIMENTAL TESTING OF KA-BAND 2D SWO BASED ON THE THERMIONIC EMISSION ACCELERATOR SATURN

Experimental studies of Ka-band 2D SWOs were performed based on the microsecond accelerator SATURN operating in a single-pulse regime. A schematic of the experiments is shown in Fig. 7(a). This accelerator is powered by a Marx generator through a forming line shaping the accelerating voltage pulse, which has a relatively long (about few hundreds nanoseconds) front. The SATURN accelerator [21] is equipped with a thermionic emission magnetron-injection gun and forms a rectilinear electron beam of tubular geometry with particles energy from 200 to 300 keV and a diameter at the cathode of 100 mm. The electron beam is focused and guided by a magnetic field that

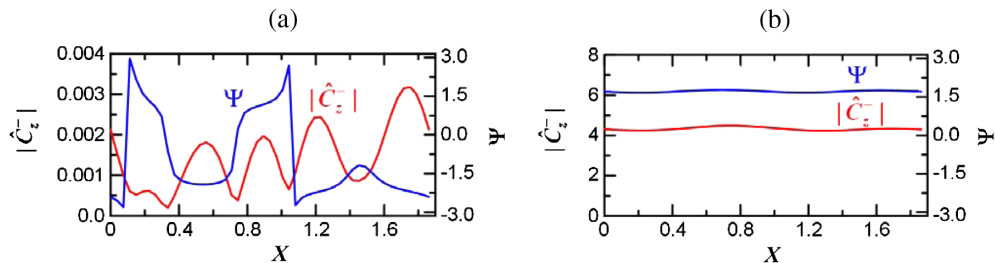


FIG. 6. Azimuthal distributions of the field amplitude $|\hat{C}_z^-|$ and phase $\Psi = \arg \hat{C}_z^-$ at the up-stream edge of SWOs at the initial (a) and the final (b) stages. Simulation parameters correspond to Fig. 5(a).

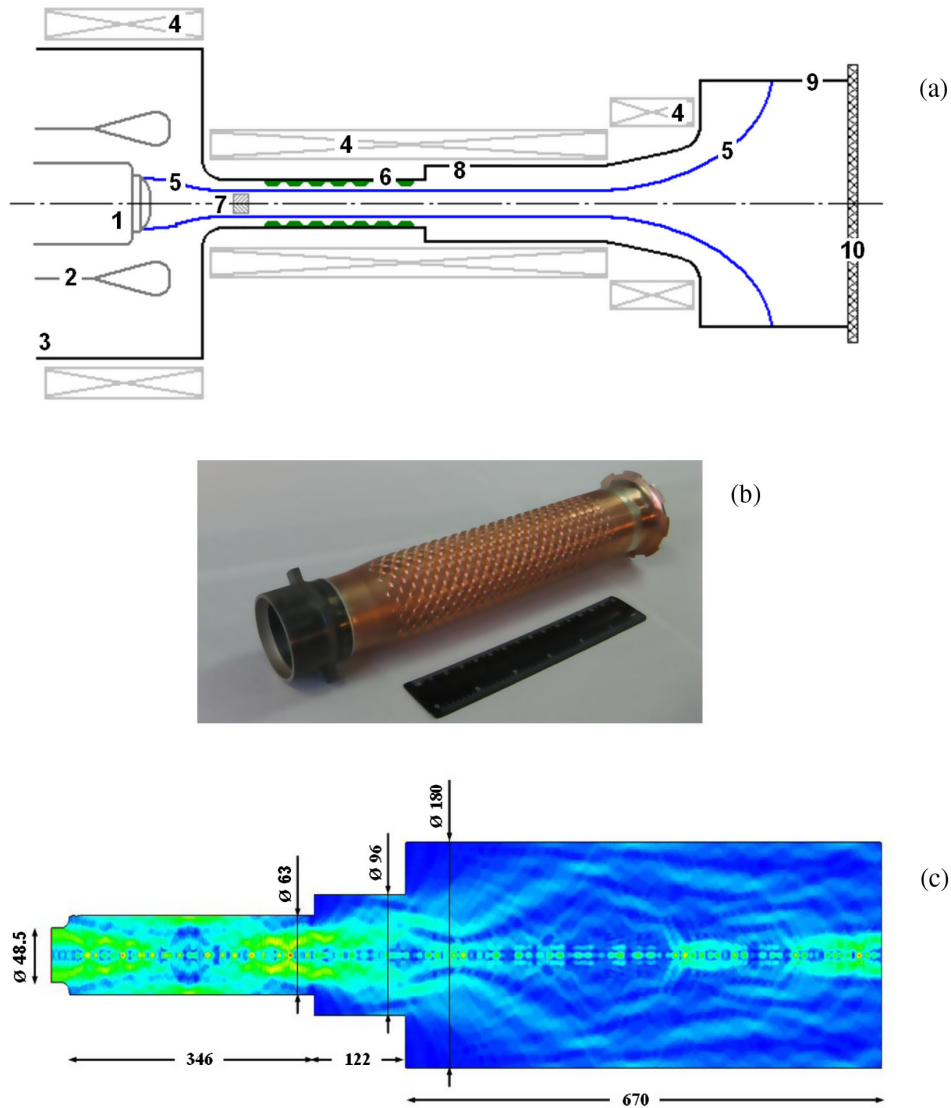


FIG. 7. (a) Scheme of experiments based on the SATURN accelerator: 1. electron beam cathode, 2. intermediate anode, 3. vacuum casing, 4. magnetic coils (solenoids), 5. electron beam trajectory, 6. slow-wave structure, 7. reflector for the radiated rf wave, 8. output section based on the Talbot effect, 9. electron beam collector, 10. output window. (b) Photograph of double periodic slow-wave structure (view outside). (c) Scheme and results of 3D simulations of the output SWO section based on the Talbot effect (geometrical sizes are given in mm).

increases from about 0.1 T at the cathode to 0.7 T at the regular part of the interaction space. As a result, inside the interaction space we have a tubular (hollow) electron beam with a diameter of 42 mm and thickness of 1 mm. The beam current was regulated by the cathode heating temperature and in this series of experiments was varied from 50 to 100 A. The beam passed into the interaction space through the annular hole between the wall of the slow-wave structure and the radiation reflector.

The 2D slow-wave structure with an oversize factor (ratio of perimeter to wavelength) of about 16 was exploited in this SWO [Fig. 7(b)]. An additional reflector of coaxial geometry was installed up-stream (cathode side) the interaction space to provide the radiation extraction from the collector side of the device. This reflector was attached to the slow-wave

structure by means of three thin radial lamellas, which (in accordance with the simulations) practically did not disturb the electron beam propagation and did not melt during the current pulse. The output section of the SWO represents an oversized circular waveguide, stepped in diameter, operating based on the Talbot effect. Such waveguide shape provides a repetition of the incident wave beam at a certain distance at the output [Fig. 7(c)].

PIC simulations of this SWO oscillator were carried out using the CST STUDIO SUITE software package. Basic simulated parameters of the slow-wave structure together with beam parameters corresponding to experimental values are given in Table I. The onset of the steady-state oscillations regime for a voltage rise time of 100 ns is shown in Fig. 8(a). High azimuthal mode was excited [Figs. 8(c) and 8(d)].

TABLE I. Basic parameters of Ka-band 2D SWOs realized on the thermionic-emission accelerator SATURN and design parameters for the project based on the high-current explosive-emission accelerator SINUS-6.

	SATURN accelerator	SINUS-6 accelerator
Mean radius of the cylindrical cavity	23 mm	
Length of the structure	210 mm	84 mm
Corrugation period	7 mm	
Number of azimuthal variations	16	
Corrugation depth	2.5 mm	
Radius of the hollow electron beam	21 mm	
Electron beam energy	200–300 keV	500–600 keV
Current	50–100 A	4–6 kA
Pulse duration	4 μ s	20 ns
Guide magnetic field	0.7 T	1.4 T

The steady-state field spectrum [Fig. 8(b)] corresponds to the frequency of the “cold” mode with an azimuthal index of $m = 3$ [compare with Fig. 3(a)].

Figure 9 shows the results of the experimental investigation of the SWO with 2D slow-wave structure based on the SATURN accelerator. In these experiments, the output

SWO power was measured by a calorimeter, the spectrum measurements were performed using a heterodyne technique. As a result, under the optimal conditions, stable narrow-band generation was obtained. In Fig. 9(a), pulses of voltage, beam current and rf signal are plotted. A comparison of the detected signal spectrum [Fig. 9(b)] with Fig. 3(a) demonstrates as well that the oscillation frequency of 32.5 GHz corresponds to the excitation of a mode with three azimuthal variations of the field as predicted by the PIC simulation (see Fig. 8). Fine pulse-to-pulse reproducibility of the oscillation spectrum was observed. Figure 9(c) shows the dependence of the oscillation frequency (spectrum line center) on the beam voltage amplitude which coincides well with the simulation results. Calorimetric measurements indicate the power level of 1.5–2 MW in up to 200 ns-long radiation pulses, which corresponds to the electron efficiency of $\sim 5\%$. Hence, experimental results conform to the theoretical analyses both within the quasioptical model and within PIC simulations.

Results of 3D simulations of electron beam dynamics in the SWO based on the SATURN accelerator are shown in Fig. 10. The simulation parameters correspond to the experimental conditions and take into account such important factors as the space charge effect, the spread of beam parameters, etc. These simulations demonstrate stable beam transportation, which is confirmed by the results of the

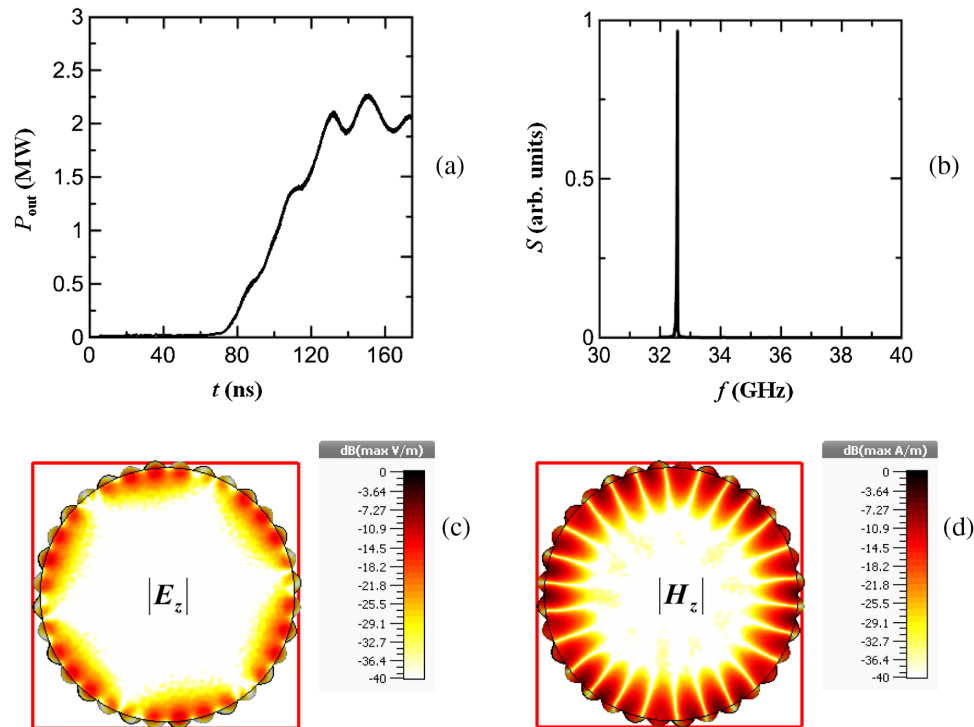


FIG. 8. Results of 3D CST PIC simulations for parameters corresponding to the experimental conditions at the SATURN accelerator: (a) Temporal dependence of the output power P_{out} , (b) rf spectrum S at the final stage of the evolution and spatial structure of the field components, (c) E_z and (d) H_z at the central cross section.

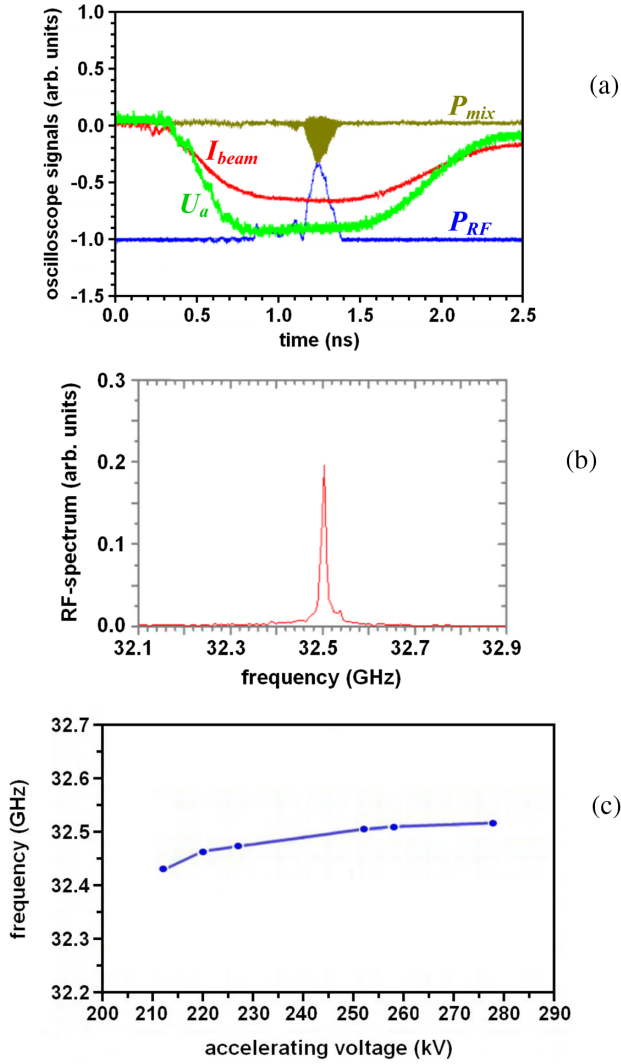


FIG. 9. Results of experimental studies of oversized Ka-band SWOs based on the SATURN accelerator: (a) typical oscilloscope traces of the accelerating voltage U_a (green curve), beam current I_{beam} (red curve), signal from a heterodyne mixer P_{mix} (brown curve) and output rf-pulse P_{rf} (blue curve); (b) spectrum of the output radiation and (c) dependence of the radiation frequency on the accelerating voltage.

experiments. Note that for the first proof-of-principle experiments, the interaction length (the length of the slow wave structure) was chosen to exceed the optimal value to deliberately ensure the excess of the starting conditions for self-excitation of the oscillator. This coincides with the results of 3D simulations, which demonstrated the possibility to enhance the output power with a certain reduction in the interaction length in the realized SWO.

Thus, we experimentally demonstrate the narrow spectrum MW-level Ka-band generation in the oversized SWOs based on 2D slow-wave structure. Nevertheless rather long voltage rise time at the SATURN accelerator does not allow for provision of azimuthally symmetric output structure of the field.

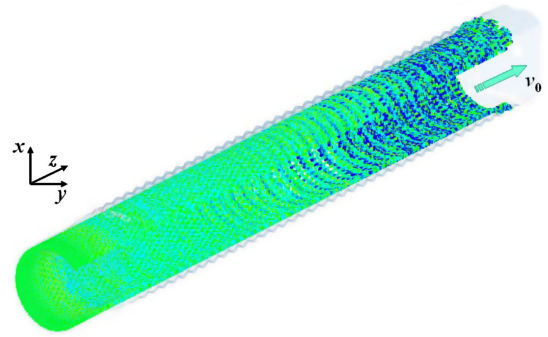


FIG. 10. Results of CST PIC simulations of the electron beam dynamics in the SWO realized at the SATURN accelerator (the electron trajectories in the stationary regime of oscillation are shown).

IV. PIC SIMULATIONS OF A KA-BAND 2D SWO BASED ON THE HIGH-CURRENT EXPLOSIVE EMISSION ACCELERATOR SINUS-6

Experiments demonstrating the possibility of obtaining stable single-mode oscillation using a 2D oversized slow-wave structure provide the potential for employing this scheme for generation from sub-GW to GW power radiation based on high-current beams formed by the explosive emission accelerators. The rather short (nanoseconds) voltage pulse front in these accelerators supplies conditions for generation at the azimuthally symmetric mode. To demonstrate the possibility of increasing output power, we conducted a PIC simulation of 2D Ka-band SWOs based on the explosive-emission accelerator SINUS-6. In this type of accelerator, the pulse shaping line is charged using a Tesla transformer with a ferromagnetic core incorporated into the line and connected to the cathode [22]. The SINUS-6 accelerator is capable of forming a wide hollow electron beam with a particle energy of 500–700 keV, a current of several kiloamperes and a duration of about 20 ns. Parameters of the corrugated waveguide (see Table I) were almost the same as those used in simulations and the experiments described above. For a Ka-band oscillator with a fairly large oversized waveguide (perimeter of about 16 wavelengths as well), a steady-state regime settled with a narrow radiation spectrum [see Figs. 11(a) and 11(b)]. Spatial structures of the excited field are shown in Figs. 12 and 13. In accordance with the theoretical considerations presented in Sec. II, these structures are the superpositions of the longitudinal C_z^\pm and the azimuthal C_x^\pm wave beams. In the simulations, one is able to separate these wave beams according to Eq. (3b): the longitudinally propagating wave beams C_z^\pm possess a nonzero E_z component of the electric field [Eq. (3b)] while the azimuthally propagating wave beams C_x^\pm have a nonzero H_z component of magnetic field [Eq. (3a)]. The steady-state distributions of E_z corresponding to the axially propagating wave beams are plotted in Figs. 12(a)–12(c). A bell-shaped structure along the longitudinal coordinate and radial decay of the fields close to the

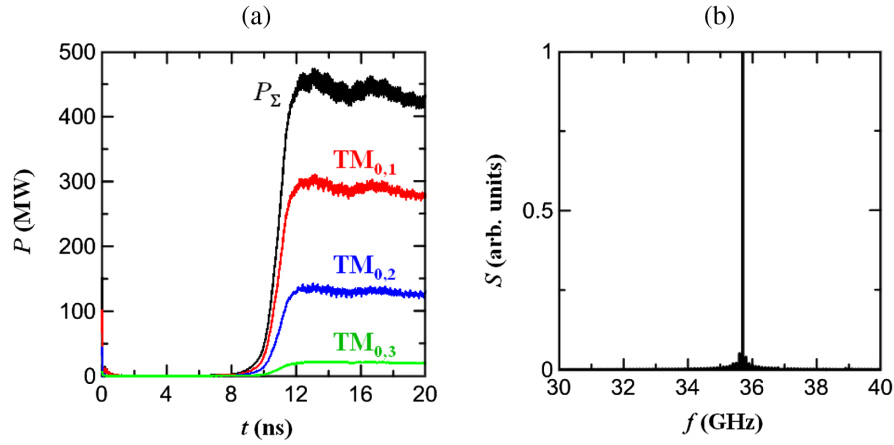


FIG. 11. CST PIC simulations of sub-GW Ka-band 2D SWOs based on the high-current accelerator SINUS-6: (a) Time dependence of the total output power P_Σ and partial powers associated with various azimuthally symmetric modes and (b) radiation spectrum S in the steady-state generation regime.

exponential is clearly seen. Beatings of the amplitude are caused by the interference of counterpropagating C_z^+ and C_z^- waves [see Eq. (3)]. With respect to the azimuthal coordinate, E_z is an azimuthally symmetric surface wave.

Expansion of it into the spectrum of modes of regular cylindrical waveguide is a combination of $TM_{0,n}$ modes. The output radiation from the oscillator [Figs. 12(c)–12(e)] has azimuthally symmetric structure as well.

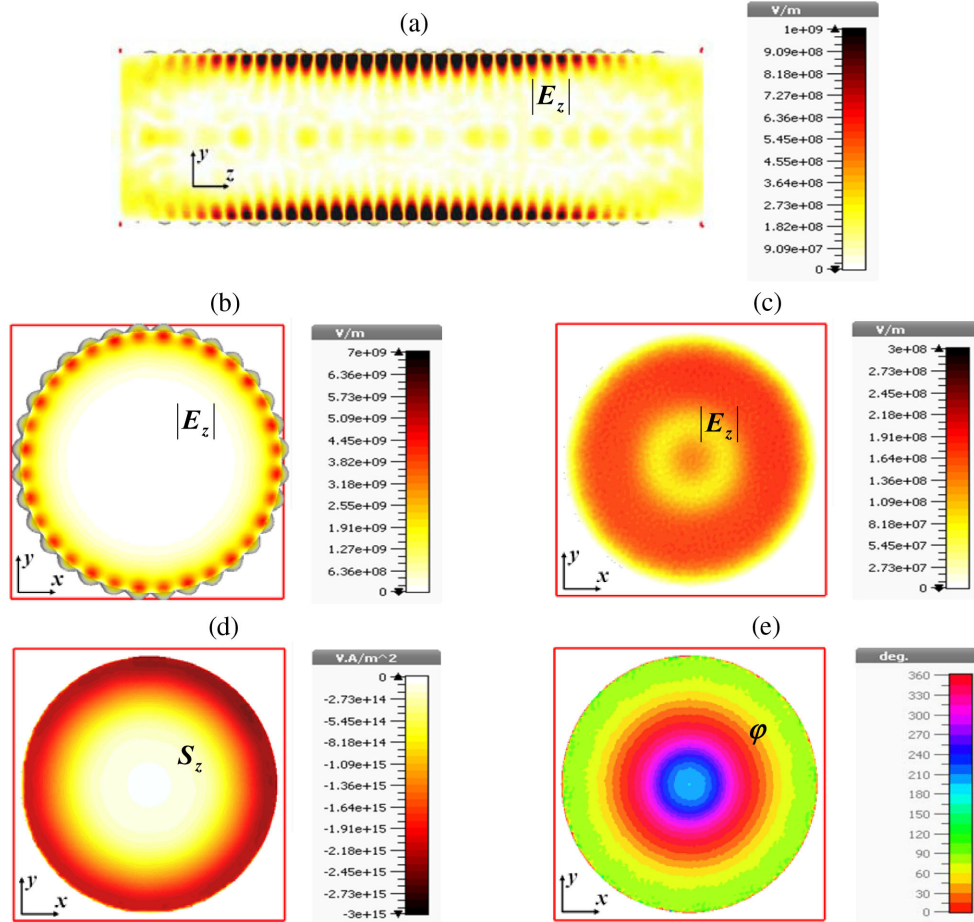


FIG. 12. CST PIC simulations of the sub-GW Ka-band 2D SWO (SINUS-6 accelerator): E_z components of the rf field, which correspond to interference of the axially propagating partial wave beams \hat{C}_z^\pm in the longitudinal (a), central (b) and output (c) cross sections of the waveguide, as well as axial component of Poynting vector S_z (d) and the phase distribution of output radiation (e).

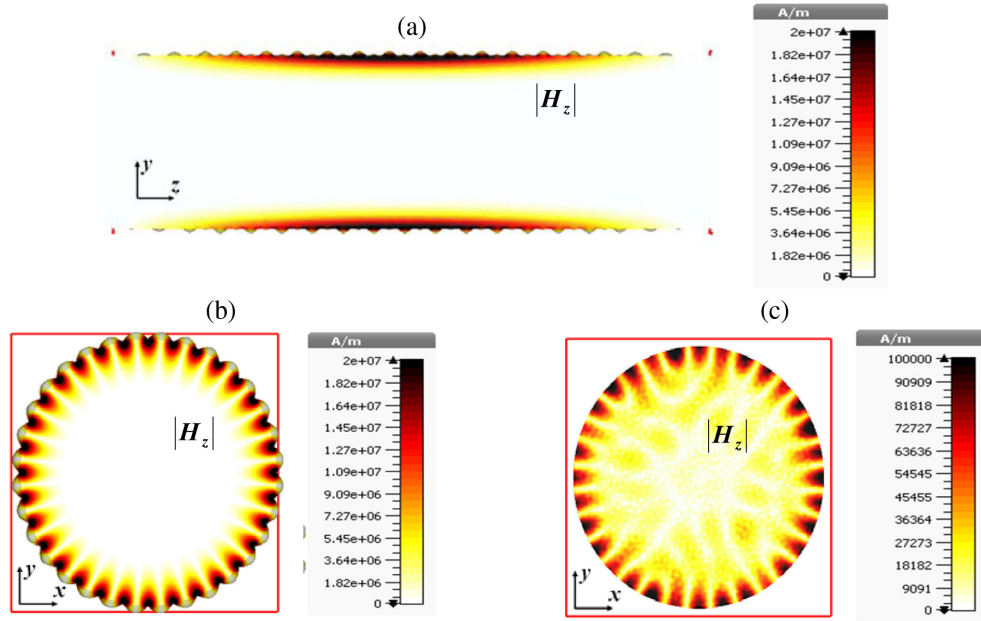


FIG. 13. CST PIC simulations of the sub-GW Ka-band 2D SWO (SINUS-6 accelerator): H_z components of the rf field, which correspond to interference of transversely (azimuthally) propagating partial wave beams \hat{C}_x^\pm in the longitudinal (a), central (b) and output (c) cross sections of the waveguide.

The longitudinal magnetic field component H_z depicted in Fig. 13 corresponds to the interference of the azimuthally propagating C_x^+ and C_x^- partial waves. As a result, a standing wave is formed along the azimuthal coordinate consisting of the counterrotating TE modes with index m

equal to the number of azimuthal variations of corrugated surface $2M$ (in the simulations $M = 16$).

Results of 3D simulations of the electron beam dynamics in this SWO are shown in Fig. 14(a). In this case, a deeper modulation of the particles energies is achieved at a relatively short interaction length [Fig. 14(b)] compared to the 2D SWO oscillator described above in Sec. III. As a result, at an operating frequency of 36 GHz, the electron efficiency could reach up to 25%, and with a total beam current of 4 kA and a particles energy of 0.5 MeV, the output power of the simulated oscillator would be as high as 400 MW.

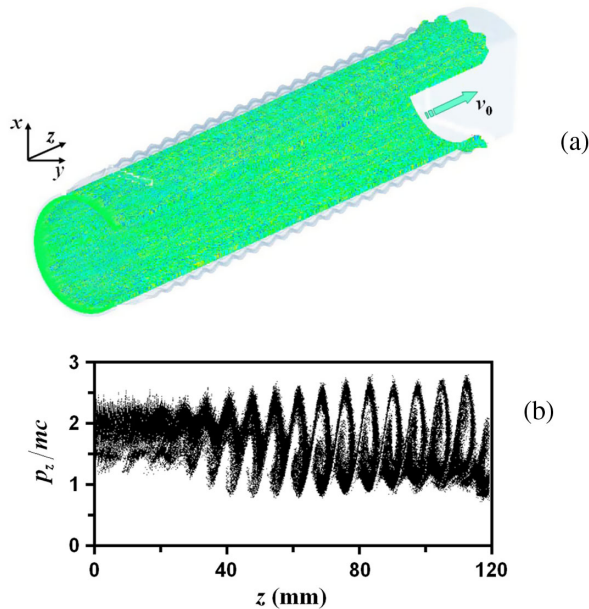


FIG. 14. Results of CST PIC simulations of the electron beam dynamics in the project of SWOs based on the SINUS-6 accelerator: (a) the electron trajectories and (b) dependence of the particles normalized momentum p_z/mc on the axial z —coordinate in the stationary regime of oscillation.

V. SUMMARY

The possibility of using 2D slow-wave structures for generation of spatially coherent narrow-band radiation in oversized cylindrical SWOs was demonstrated. The presence of the azimuthally propagating wave beams formed by the 2D structure leads to a substantial rarefaction of the spectrum of modes with different azimuthal indices thus allowing their selective excitation by a large-size rectilinear hollow electron beam. For longer (hundreds nanoseconds to microseconds) voltage rise time, the modes with high azimuthal indices are excited. These conclusions are supported by the experiments where the Ka-band 2D SWO was realized based on the thermionic accelerator SATURN (300 keV/100 A/4 μ s). For a fairly large oversize factor (up to 16), stable narrow-band generation with an output power of 1.5–2 MW was obtained at the frequency of 32.5 GHz corresponding to excitation of the third azimuthal mode. The project of Ka-band 400 MW power SWOs based on the high-current explosive-emission accelerator SINUS-6

(500 keV/4 kA/20 ns) operating at the azimuthal symmetric mode is developed. According to the simulations, the total power of Cherenkov SWOs with 2D slow-wave structure would substantially exceed the power of a FEM with the 2D Bragg resonator [3–5] due to the possibility of using more intense rectilinear electron beams.

ACKNOWLEDGMENTS

This work is partially supported by the Russian Foundation for Basic Research (Grants No. 16-02-00890 and No. 16-08-00811) in the part of theoretical and experimental studies of 2D SWOs based on the SATURN accelerator and the Russian Government Project No. 0035-2014-0012 in the part of the design of sub-GW SWO oscillators.

-
- [1] N. S. Ginzburg, N. Yu. Peskov, and A. S. Sergeev, Dynamics of free-electron lasers with two-dimensional distributed feedback, *Opt. Commun.* **112**, 151 (1994).
- [2] N. S. Ginzburg, N. Yu. Peskov, A. S. Sergeev, V. Yu. Zaslavsky, I. V. Konoplev, L. Fisher, K. Ronald, A. D. R. Phelps, A. W. Cross, and M. Thumm, Mechanism of azimuthal mode selection in two-dimensional coaxial Bragg resonators, *J. Appl. Phys.* **105**, 124519 (2009).
- [3] I. V. Konoplev, A. W. Cross, A. D. R. Phelps, W. He, K. Ronald, C. G. Whyte, C. W. Robertson, N. S. Ginzburg, N. Yu. Peskov, A. S. Sergeev, V. Yu. Zaslavsky, and M. Thumm, Experimental and theoretical studies of a coaxial free-electron maser based on two-dimensional distributed feedback, *Phys. Rev. E* **76**, 056406 (2007).
- [4] A. V. Arzhannikov, N. S. Ginzburg, V. Yu. Zaslavsky, V. G. Ivanenko, I. A. Ivanov, P. V. Kalinin, A. S. Kuznetsov, S. A. Kuznetsov, N. Yu. Peskov, A. S. Sergeev, S. L. Sinitsky, and V. D. Stepanov, Generation of spatially coherent radiation in free-electron masers with two-dimensional distributed feedback, *JETP Lett.* **87**, 618 (2008).
- [5] A. V. Arzhannikov, N. S. Ginzburg, P. V. Kalinin, S. A. Kuznetsov, A. M. Malkin, N. Yu. Peskov, A. S. Sergeev, S. L. Sinitsky, V. D. Stepanov, M. Thumm, and V. Yu. Zaslavsky, Using Two-Dimensional Distributed Feedback for Synchronization of Radiation from Two Parallel-Sheet Electron Beams in a Free-Electron Maser, *Phys. Rev. Lett.* **117**, 114801 (2016).
- [6] N. S. Ginzburg, V. Yu. Zaslavsky, A. M. Malkin, N. Yu. Peskov, and A. S. Sergeev, Cherenkov masers with two-dimensional distributed feedback, *Tech. Phys. Lett.* **36**, 83 (2010).
- [7] I. V. Konoplev, A. J. MacLachlan, C. W. Robertson, A. W. Cross, and A. D. R. Phelps, Cylindrical periodic surface lattice as a metadielectric: Concept of a surface-field Cherenkov source of coherent radiation, *Phys. Rev. A* **84**, 013826 (2011).
- [8] N. S. Ginzburg, E. V. Ilyakov, I. S. Kulagin, N. Yu. Peskov, R. M. Rozental, A. S. Sergeev, V. Yu. Zaslavsky, and I. V. Zheleznov, Synchronization of radiation in an oversized coaxial Ka-band backward wave oscillator using two-dimensional Bragg structure, *Phys. Rev. ST Accel. Beams* **18**, 120701 (2015).
- [9] A. R. Phipps, A. J. MacLachlan, C. W. Robertson, L. Zhang, I. V. Konoplev, A. W. Cross, and A. D. R. Phelps, Electron beam excitation of coherent sub-terahertz radiation in periodic structures manufactured by 3D printing, *Nucl. Instrum. Methods Phys. Res., Sect. B* **402**, 202 (2017).
- [10] V. L. Bratman, G. G. Denisov, M. M. Ofitserov, S. D. Korovin, S. D. Polevin, and V. V. Rostov, Millimeter-wave HF relativistic electron oscillators, *IEEE Trans. Plasma Sci.* **15**, 2 (1987).
- [11] S. P. Bugaev, V. A. Cherepenin, V. I. Kanavets, V. I. Koshelev, V. A. Popov, and A. N. Vlasov, Investigation of a millimeter-wavelength-range relativistic diffraction generator, *IEEE Trans. Plasma Sci.* **18**, 518 (1990).
- [12] J. Urata, M. Goldstein, M. F. Kimmitt, A. Naumov, C. Platt, and J. E. Walsh, Superradiant Smith-Purcell Emission, *Phys. Rev. Lett.* **80**, 516 (1998).
- [13] A. N. Vlasov, A. G. Shkvarunets, J. C. Rodgers, Y. Carmel, T. M. Antonsen Jr., T. M. Abuefadi, D. Lingze, V. A. Cherepenin, G. S. Nusinovich, M. Botton, and V. L. Granatstein, Overmoded GW-class surface-wave microwave oscillator, *IEEE Trans. Plasma Sci.* **28**, 550 (2000).
- [14] H. L. Andrews and C. A. Brau, Gain of a Smith-Purcell free-electron laser, *Phys. Rev. ST Accel. Beams* **7**, 070701 (2004).
- [15] Y. M. Shin, J. K. So, K. H. Jang, J. H. Won, A. Srivastava, and G. S. Park, Evanescent Tunneling of an Effective Surface Plasmon Excited by Convection Electrons, *Phys. Rev. Lett.* **99**, 147402 (2007).
- [16] C. Prokop, P. Piot, M. C. Lin, and P. Stolz, Numerical modeling of a table-top tunable Smith-Purcell terahertz free-electron laser operating in the super-radiant regime, *Appl. Phys. Lett.* **96**, 151502 (2010).
- [17] S. Gong, K. Ogura, K. Yambe, S. Nomizu, A. Shirai, K. Yamazaki, J. Kawamura, T. Miura, S. Takanashi, and M. T. San, Experimental study of intense radiation in terahertz region based on cylindrical surface wave resonator, *J. Appl. Phys.* **118**, 123101 (2015).
- [18] G. Wang, J. Wang, P. Zeng, S. Li, and D. Wang, Overmoded subterahertz surface wave oscillator with pure TM_{01} mode output, *Phys. Plasmas* **23**, 023104 (2016).
- [19] N. S. Ginzburg, A. M. Malkin, A. S. Sergeev, and V. Yu. Zaslavsky, Powerful surface-wave oscillators with two-dimensional periodic structures, *Appl. Phys. Lett.* **100**, 143510 (2012).
- [20] N. S. Ginzburg, A. M. Malkin, A. S. Sergeev, and V. Yu. Zaslavsky, Oversized co-axial and cylindrical surface-wave oscillators with two-dimensional periodical grating (quasi-optical model), *J. Appl. Phys.* **113**, 104504 (2013).
- [21] N. I. Zaitsev, E. V. Ilyakov, G. S. Korablyov, I. S. Kulagin, V. K. Lygin, B. Z. Movshevich, V. I. Tsalolikhin, and M. Yu. Shmelev, High-current microsecond electron accelerator with a thermocathode for power SHF instruments, *Instrum. Exp. Tech.* **38**, 380 (1995).
- [22] S. D. Korovin and V. V. Rostov, High-current nanosecond pulse-periodic electron accelerators utilizing a tesla transformer, *Russ. Phys. J.* **39**, 1177 (1996).